On the role of Sc in powders and spray deposits of hypoeutectic Al-Cu

H. Henein[1], A-A. Bogno[1], S. Yin[1,2], P. Natzke[1], M. Gallerneault[2]

[1]Department of Chemical and Materials Engineering, University of Alberta
Edmonton, Alberta, Canada T6G 1H9

[2]Department of Mechanical and Materials Engineering, Queen's University, Kingston, Ontario, Canada K7L 3N6

Key words: Undercooling, atomization, powders, spray deposition, Al-Cu, scandium, solidification microstructures

Abstract

Scandium (Sc) is an expensive alloying element which has an important effect on the properties of aluminum alloys. It is of interest to determine for a variety of solidification conditions the effect of minor addition, in the hypoeutectic levels, of Sc on Al alloys. This study builds on past work on rapid and slow solidification of Al-4.5Cu-0.4Sc (wt%) by comparing previous microstructures to those obtained using spray forming of strip. The effect of Sc (0.4wt%) on the scale of the microstructure of as-atomized powders and as-deposited strips (SD) is found to be negligible in the investigated alloys. The eutectic undercooling of the Al-4.5Cu-0.4Sc (wt%) alloy is the same for both powders and SD. This is attributed to eutectic nucleation and growth following the same path in both solidification processes, characterized by an extended solubility of Sc in the primary α-Al matrix, as evidenced by the resulting Sc-rich precipitates and inherent age hardening upon annealing of the as-solidified samples. This work contributes to building an understanding of rapidly cooled structures and their subsequent self-aging in advanced manufacturing processes.

Graphical Abstract

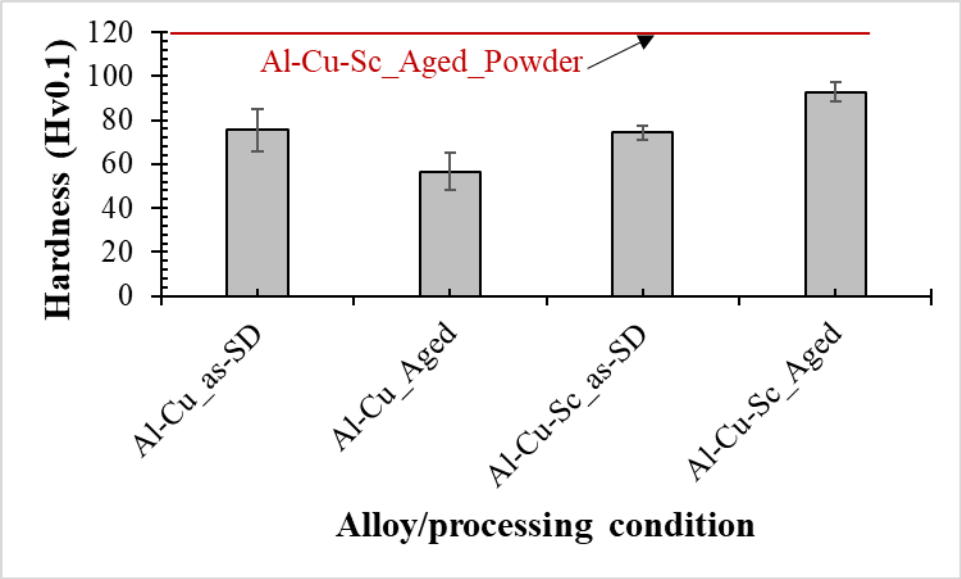

Microhardness comparison of as solidified spray formed strip of Al-Cu and Al-Cu-Sc with spray formed and aged alloys.

Funding details

This work was supported by NSERC Strategic Grants program.

Disclosure Statement

The authors report no competing interests to declare.

1. Introduction

Solidification processing has a strong effect on the mechanical properties of alloys. Variations in solidification conditions, such as undercooling and / or cooling rate, gives rise to the ability to control microstructure size, morphology, and amounts and types of phases. These will affect the physical and chemical properties of metallic alloys. High cooling rates and large nucleation undercoolings induce rapid solidification and can result in reduced microsegregation and often in the formation of a range of metastable microstructures [1].

To attain high solidification undercooling , it is necessary to minimize the nucleation potential of the melt. Containerless solidification techniques have been developed to minimize nucleation induced by impurities from melt container walls [2]. Drop tubes are one of the most reliable containerless solidification techniques and have been used to analyze rapid solidification microstructures of a wide range of metallic alloys [3-11]. In this work, the Impulse Atomization (IA) drop tube was used. Using mechanical impulses IA creates liquid ligaments that break-up and spheroidize into droplets that solidify by rapidly losing heat as they fall under gravity through a stagnant gas of choice (Ar, He, N_2, etc.). The technique provides not only containerless solidification advantages but through the atomization of the melt, the droplets are small and isolated and thus the number of nucleation sites are significantly reduced. As has been demonstrated in other works [12-14], a higher level of undercooling would occur as the atomized droplets solidify rapidly into powders. Alternately, the droplets may be deposited and finally solidify on a substrate while semi-solid in which case the term Spray Deposition (SD) is used [3]. The oxygen concentration in the atomization chamber is usually maintained at a minimum possible level (e.g. 20ppm). However, the oxygen partial pressure at such levels (~70 mbar) is not sufficient to protect the droplets from forming an aluminum oxide layer on the powder surface [15] as they fall. Thus, most of the semi solid SD droplets are isolated from each other by the oxide layers in an SD deposit. As a result, nucleation of subsequent phases during further solidification occurs in isolation in each of these droplets. This, results in extended solid solubility and eutectic undercooling [16]. Thus, IA offers a unique means

to achieve far-from-equilibrium microstructures through high cooling rates and large undercoolings for both powders and SD. Such an approach was used to study the SD of two AlMgSc alloys. [17]

Aluminum alloys are widely used in the automobile and aerospace industries as they have high specific strength (density), excellent corrosion resistance and good formability [18]. The addition of transition metals (TM), such as Cu or Sc, result in the formation of supersaturated solid solution during rapid solidification from which substantial age hardening is possible, and high cooling rates and high nucleation undercooling increases the solubility of transition metals in solid aluminum. This applies particularly to eutectic solidification undercooling. The use of atomization of melts leads to high cooling rate and undercooling and has led to many investigations into Al-TM alloys.

Hypoeutectic additions of Sc to Al-Cu alloys is reported to strengthen them through age hardening [19]. Supersaturation of Sc in the aluminum matrix is required to reach good aging performance [20]. For traditional Direct Chill (DC) casting, only low cooling rates in the range of 1°C/s to 10°C/s can be achieved [21]. With such low cooling rates, the supersaturation of Sc can only be obtained through homogenization or solutionising and quenching. Since Sc has a low solubility and diffusivity in aluminum, this process is carried out at high aluminum-processing temperatures (~500°C) for a relatively extended period of time (~20 hours) [22].

In this work, IA is used to generate rapidly solidified Al-4.5wt% Cu-xSc (x= 0.0 or 0.4wt%) powders and strips. Using this technique, we generate several droplets during a single experimental run, droplets that can be collected as rapidly solidified powders or as a SD strip. In the case of SD strip, we impact them on to a moving substrate while they are still partially molten. Thus, by varying the droplet size, gaseous atmosphere and superheating [4, 5], tailored microstructures can be obtained. This paper studies the effects of IA, and

SD induced rapid solidification on the resulting microstructures (cell spacing) and mechanical properties (hardness and yield strength) of hypoeutectic Al-Cu-Sc.

2. Materials and methods

2.1. Materials

Al-4.5wt% Cu-xSc (x= 0.0, and 0.4wt% Sc) droplets generated by IA were rapidly solidified from various melt temperatures in Ar atmosphere; measured oxygen levels in the chamber were no greater than 20 ppm. A detailed description of this process is given elsewhere [6] [17] [23]. In this study, 350 grams of each investigated chemistry, pre-alloyed to the composition of interest, were heated to 200˚C above the alloy liquidus temperature.

Powders were obtained by collecting the rapidly solidified droplets 4 m below the atomization orifices in an oil filled beaker. The droplets were fully solid before reaching the oil bath.

Strips were obtained by a spray deposition (SD) process [3]**,** during which, the atomized droplets of median diameter (D50) around 350µm, in a mushy state (partially solidified) were made to land, 0.4 m below the atomization orifices, on a 3 mm thick copper substrate, moving at 0.038ms^{-1}. A detailed description of the substrate assembly for SD is presented elsewhere.[17]

The substrate is mounted, through a support, on a belt driven linear carriage/guide system, which was connected to a stepper motor (motor with cooling system) to ensure a controlled, reproducible substrate speed. The maximum displacement of the moving carriage was 650mm. A heating element is sandwiched between the substrate and its support to preheat the substrate in order to remove any adsorbed water vapor. In the present work, prior to SD, the copper substrate was preheated, and its temperature was 100 ºC when the semi solid droplets spray landed upon it. A thin layer of oil coating was applied to the substrate surface to give better contact between the deposit and the substrate. In this paper, the suffix "-wo" (with oil) is added in the legends, to label the samples generated on the oil coated substrate and distinguish them from the rest. A schematic description of the SD experimental setup is found elsewhere [24]. Figure 1 shows a photo of atomized powder and strip after a single pass of the substrate movement.

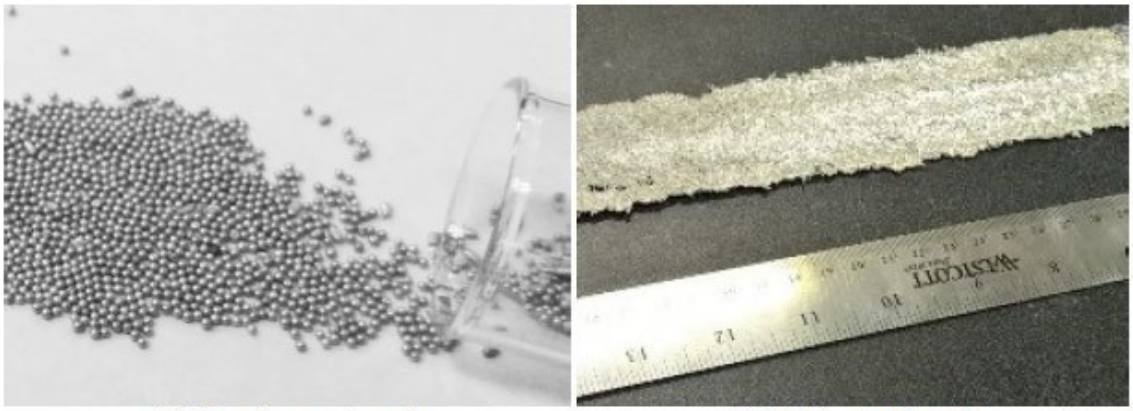

(a) Powder produced (b) Strip produced

Figure 1: Atomized Al-4.5wt%Cu (a) powders and (b) SD.

Applying the above-described techniques, powders and strips with different thermal histories were generated for this study (Table 1).

Table 1. Summary of the investigated samples

Nominal Composition [wt%]	**T_{inital} [°C]**	**Type of sample**	**Orifice Diameter [μm]**
Al-4.5Cu	850	Powder	350
		SD Strip	350
Al-4.5Cu-0.4Sc		Powder	350
		SD Strip	350

A mathematical model was used to describe the thermal profile of atomized droplets in flight [4, 5]. The thermal model relates the distance of the droplets from the nozzle orifice to the temperature and solid fraction of the droplets. For the strip, the temperature was monitored with a system for the top and bottom of the strip. The top surface of the strip was measured using an emissivity probe, Mikron QL3600C-2B. To ensure that an inert atmosphere was maintained in the SD chamber while IR measurements were taken, a 75 mm diameter Germanium lens with 3-12 mm AR coating was used as a window. This ensures that there is no absorption by the window of IR signal emitted from the strip and received by the IR camera. For the bottom of the strip, a two color pyrometer was used to

measure the temperature of the bottom surface of the deposited strip. A small hole (0.55mm in diameter) was drilled through the substrate (0.9mm thick). A two color pyrometer, LumaSense ISR 12-LO, was used. This pyrometer is able to read a spot size as small as 0.45mm at a focal distance of 87 mm.

2.2. Microstructural Characterization

2.2.1. Microscopy

Microstructural examination of the powders and the SD was done using Scanning Electron Microscopy (SEM, A Tescan Vega3) and Optical Microcopy (OM, a motorized BX61 Olympus microscope). The size of the solidified structure was measured following ASTM E112-13. SEM equipped with an energy dispersive X-ray (EDX) analysis system (INCA Microanalysis System, Oxford Instruments) was used. To provide atomic number (Z) contrast, imaging was done in backscattered electron (BSE) mode, at an accelerating voltage of 10 kV for both powders and strip samples. Prior to microscopy, the samples were mounted in epoxy resin, ground, and polished, (then etched with Keller's reagent for 10-20s for OM).

For intermetallic precipitates, *Electron backscatter diffraction (*EBSD, a Zeiss Sigma 300 VP-Field Emission Scanning Electron Microscope (FE-SEM)) was used.

2.2.2. Cell spacing, hardness, and strength evaluation

The average secondary dendrite arms spacing, or cell spacing, defined as the center-to-center distance between two dendritic cells, was measured using the linear line intercept method (ASTM E112-13). This microstructural length scale will be referred to as cell spacing in this paper.

The mechanical properties were evaluated with Vickers microhardness (Buehler VH3100 microhardness tester) measurements of both the as-atomized (powders and strips), and heat-treated samples using a calibrated steel block (~62.5 Hv). At least five indentations, were randomly applied to each sample with a load of 100 gf for a holding time of 10 s. This ensured that an indentation was sufficiently large to measure across many dendritic cells.

The samples were examined following the hardness measurements to ensure the validity of the test. The measured Vickers microhardness values (H_V) were subsequently converted to ultimate tensile strength (UTS) by applying the correlation given in equation 1, which was developed for ductile metals of young modulus E ≈ 70 GPA such as the alloy 6061 [25].

$$UTS = 3.07Hv - 4.32 \quad (1)$$

2D measurements were used to quantify the eutectic volume fractions (V^e) on both powders and strips microstructures [26]. Subsequently, V^e is converted into weight percent eutectic (W^e) following equation 2.

$$W^e = \frac{V^e \times \rho_e}{V^e \times \rho_e + V^\alpha \times \rho_\alpha} \quad (2)$$

The densities of the eutectic structure and the α-phase, ρ_e and ρ_α, respectively, are obtained from the elemental weight percent of the eutectic structure measured by point-located Energy Dispersive X-ray spectroscopy (EDX). The densities of Al and Cu are ρ_{Al}=2700 kgm^{-3} and ρ_{Cu}=8920 kg m^{-3} [27].

Metastable extensions of solidus and liquidus lines on the Al-Cu phase diagram were used to determine eutectic nucleation undercooling. This was carried out by using the level rule at different undercooled eutectic temperatures until the measured eutectic fraction agreed with the lever rule calculation. The eutectic nucleation undercooling was then combined with a simple coarsening model of secondary dendrites spacing to determine the solidification interval and consequently the primary phase nucleation undercooling. A detailed description of the steps is given elsewhere [28].

2.3. Aging treatment

Standard heat treatment of Al alloys requires the heating of the alloy into a single phase region on the phase diagram in order to dissolve all solute elements into the stable solid solution, α-Al phase (solutionising). Quenching the alloy leads to solute supersaturated α-

Al. Dry ice may be used for the quenching operation. Then, a driving force triggers precipitation of equilibrium intermetallics, from the supersaturated solid solution.

Aging of Al-Cu-Sc powders and SD strip in this study were carried out following the procedure described in [19]. No solutionizing and quenching steps were used. The aging process consisted in heating the as solidified samples, in an air-furnace, up to 300°C and holding for 20hrs before water quenching them to room temperature in order to minimize solid state coarsening of the precipitates.

3. Results and Discussions

3.1. Thermal cooling rate of strip

The measured temperature and emissivity of the surface of the strip is shown in Figure 2a. The temperatures of the droplets as they land on the substrate is shown to be at a steady state of 594°C and an emissivity of 0.62. The thermal model of droplet cooling provides a temperature of droplets at this position of 600°C. The results of the two color pyrometer are shown in Figure 1b. After about 20 s, steady state is established for the surface temperature at the bottom of the strip. Between 20 and 70 s, the temperature of the bottom of the strip changes by about 20°C and has an average of 372°C. This yields a thermal gradient in the strip of 32 °C/mm as it is deposited. This is indicative of the slow thermal cooling rate of the strip.

3.2. Solidification cooling rates and microstructural length scales

Figure 3a and Figure 3b shows SEM backscattered electron (BSE) micrographs representing, respectively, typical surface and cross section microstructures of the samples (powders and SD). The micrographs in Figure 3a and Figure 3b show evidence of two types of regions characterized by different grey levels. The dark regions are Al-rich matrix (α-phase), and the white regions are the eutectic structure, consisting of Cu-rich θ-Al_2Cu + α-Al.

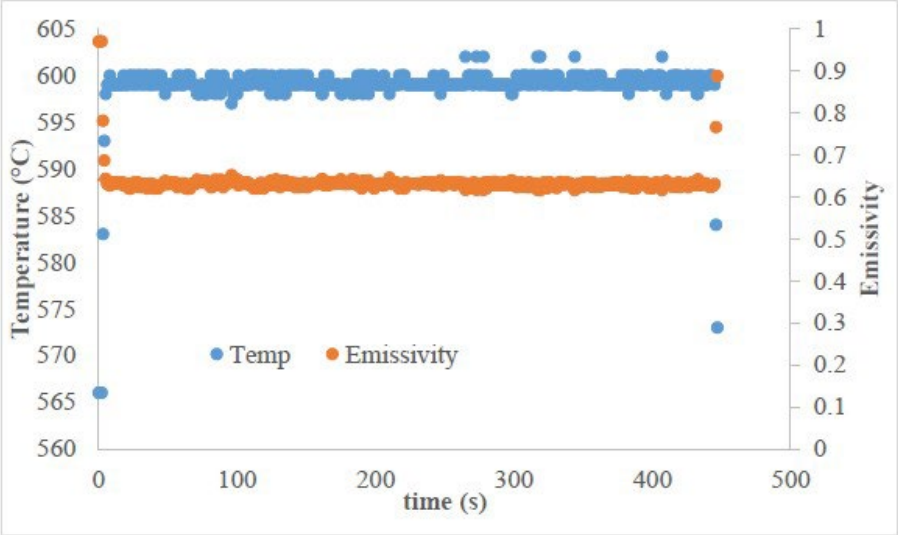

(a)

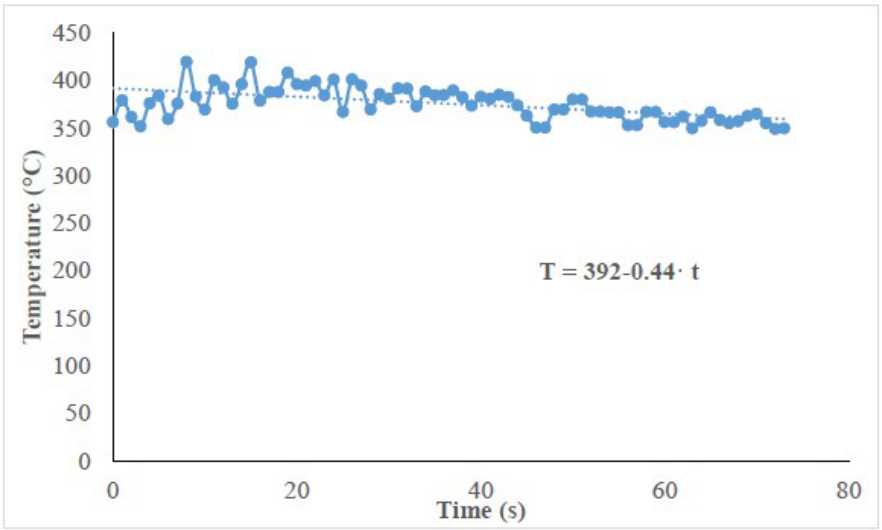

(b)

Figure 2: (a) emissivity probe reading of droplet temperature as they land on the substrate, (b) two color pyrometer reading at the bottom surface of the strip.

Since the microstructures consist of dendritic cells (α-phase), the cooling rates were estimated by the empirical expression of the secondary dendrite arm spacing ($\lambda=85\dot{T}^{-0.35}$) of Al-4.5wt% Cu-xSc (x varying from 0.0wt%Sc to 0.4wt%Sc) samples resulting from cooling rates of three different order of magnitudes generated by IA, DSC and

Electromagnetic Levitation (EML) [19]. Figure 4 shows the cell spacing variation with cooling rate for both powders and strips of both investigated Al-Cu-Sc alloys. As expected, the cell spacing decreases as the cooling rate increases. Sc has no refining effect on the microstructure, which confirms the results obtained in other publications [19, 29]. As expected, the cell spacings of the strips are larger (one order of magnitude) than those of the powders. Actually, the micron-sized droplets undergo a much higher cooling rate when they completely solidify by losing heat to the quiescent surrounding gas after atomization. Whereas, during SD, the partially liquid droplets, when they land on the copper substrate must be cooled further before the remaining liquid reaches the eutectic composition, thus increasing the coarsening time.

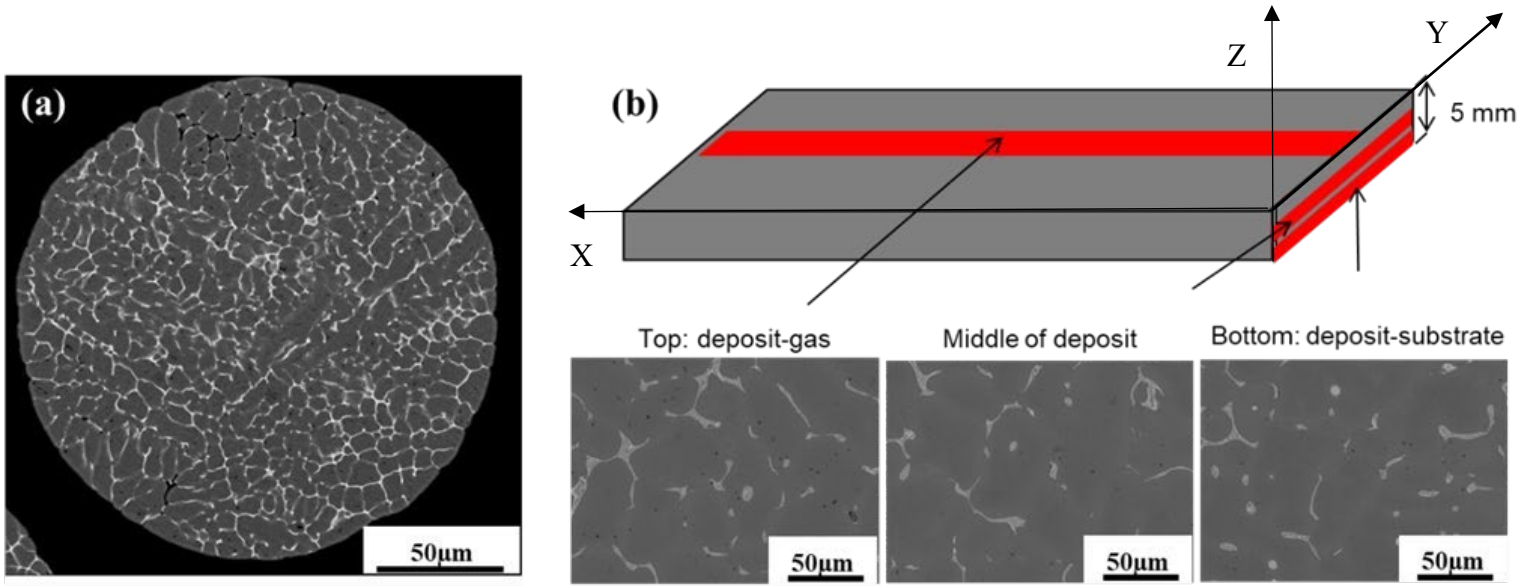

Figure 1: SEM (BSE) of typical microstructures of an impulse atomized (a) powder and (b) strip. Alloy: Al-4.5wt%-0.4wt%Sc, average size: 350µm, atomization atmosphere: Ar. The dark contrast is the α-Al and the bright contrast is the Cu-rich eutectic structure.

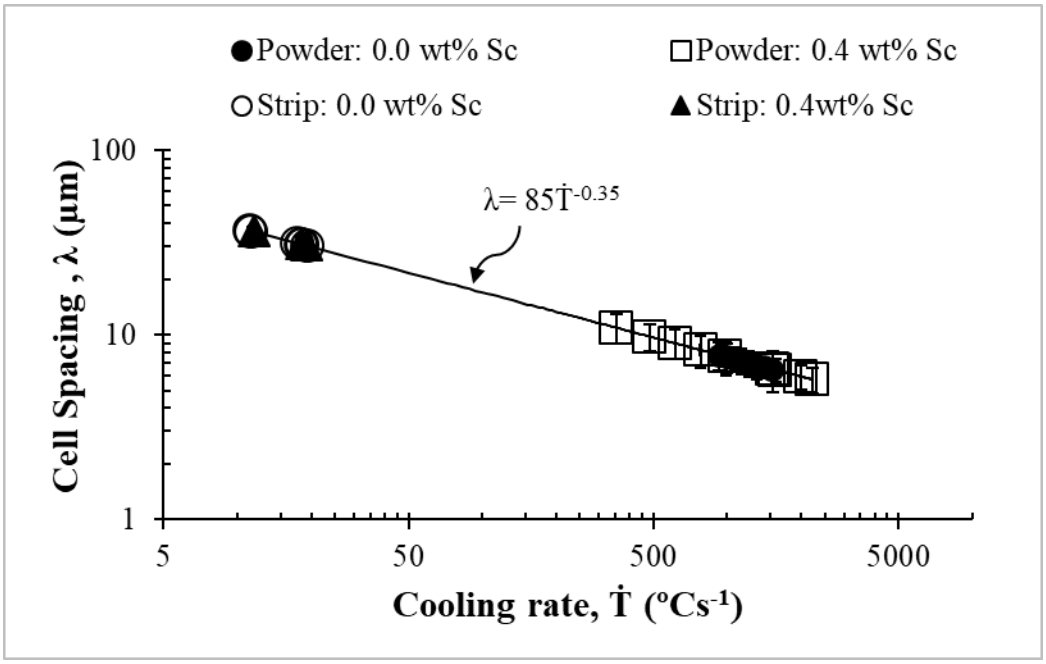

Figure 2: Variations of average cell spacing of powders, and strips microstructures of different alloy composition as a function of cooling rate. All samples were generated under argon atmosphere.

Moreover, during SD, the top surface is cooled by convective heat loss to the surrounding gas, the middle section by heat conduction to the upper and lower surfaces of the deposit, and the bottom surface is cooled by heat conduction through the copper substrate. These differences in heat transfer within a strip, will lead to different solidification cooling rates and consequently different cell spacing, depending on the location across a strip cross section.

Figure 5 shows the cell spacing variation for both Al-4.5wt% Cu-xSc strips (strip: 0.0wt%Sc and strip: 0.4wt%Sc). It can be seen that the average cell spacing is larger in the middle of the strip, which should correspond to the lowest cooling rate region. The middle section of a deposit not only receives additional heat from the falling droplets pileups, but also heat from that section is not directly transferred to the surrounding gas or to the substrate [29]; instead, it must transfer, by conduction, through the top and bottom layers of the deposit. Consequently, the heat transfer rate from the middle of the deposit is the

lowest, hence, it yields the largest cell spacing. This situation would be similar to that experienced by a deposit in an additive manufacturing process that involves the building of a component layer by layer.

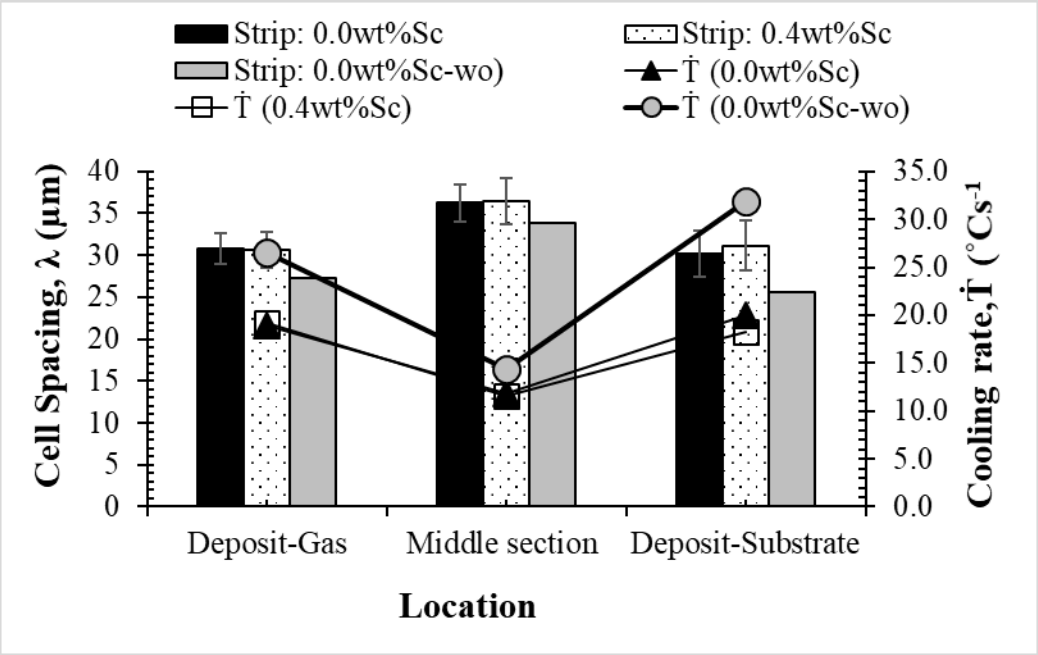

Figure 5: Variations of average cell spacing and solidification cooling rate of the strips microstructures of different alloy compositions as a function of the location of the sample cross section along Z-axis. All samples were generated under argon atmosphere. The "wo" designation indicates a spray deposition on an oil coated substrate.

3.3. Eutectic Fraction

Figure 6 shows the eutectic fraction (in wt %) of the Al-4.5wt%Cu-xSc (x=0.0wt%Sc and x=0.4wt%Sc) strips, measured at different locations from the sample cross section along Z-axis (the thickness). Despite the variation of solidification cooling rate (see Figure 5) from top to bottom, the eutectic fraction is found to be the same throughout the investigated cross-sectional areas, and equal to the eutectic fraction of a powder of 350μm in diameter, which, as mentioned earlier, is the estimated value of the median diameter, D50, of the atomized deposited spray [24]. This result suggests that eutectic fraction is nucleation undercooling dependent rather than cooling rate dependent. This occurs as the eutectic in each oxide coated slushy droplet in the deposit must nucleate its own θ-phase independent

of others adjacent to it [16]. Thus, there is extended solubility of Cu and Sc in the SD strips like that experienced in the powders. In addition, as expected for high undercooling induced rapid solidification, the estimated eutectic fractions are lower than the values predicted by the well-known Gulliver-Scheil model.

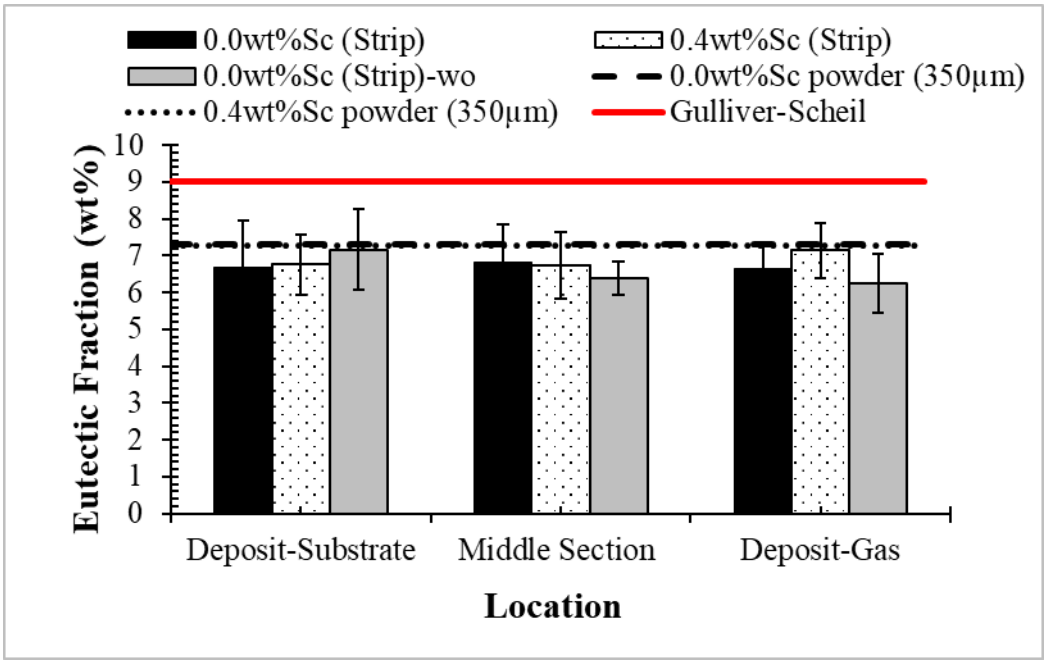

Figure 6: Weight percent eutectic at different locations of the sample cross section along Z-axis, compared with powders of equivalent size and the Gulliver-Scheil model prediction for the two investigated Al-4.5wt%Cu-xSc (x=0.0wt%Sc and x=0.4wt%Sc) alloys.

3.4. Nucleation undercooling

Eutectic undercooling results from bottom to top of the deposit's cross-sections are shown in Figure 7a. Since the D50 of the atomized droplets is 350µm, the SD results are compared to this average droplet size of the same composition. Clearly from Figure 7a, the eutectic undercooling does not vary much across the SD sample cross section from bottom to top. However, within the measurement errors, the eutectic nucleation undercooling is slightly higher in strips as compared to powders. The eutectic undercooling is rather equivalent to droplets that have a solidification cooling rate between 3500 to 10^4 Ks^{-1} [31].

Figure 7b shows the primary undercooling variation from different locations on the sample cross section along Z-axis. As can be seen, the primary undercooling remained quasi-

constant throughout the sample thickness. The values are affected by neither the cooling rate (oil coating) nor the Sc-addition. Also, the primary undercooling is found, as expected, to be consistent with a 350μm droplet size of the same composition corresponding to the D50 of the deposited spray.

After atomization and before the semi-solid droplets impact the substrate, the liquid droplets undercool, leading to the nucleation of the primary α-Al phase during the flight of the droplets. Hence, for the same composition, the primary undercooling is the same for a 350μm droplet as well as for a spray deposition consisting of droplets with sizes distributed around a 350μm D50.

On contacting the substrate, the spray generally consists of partially solidified droplets (as is the case of the investigated 350μm droplets size) as well as fully solidified and fully liquid droplets, depending on their sizes. The fully liquid droplets spread on the substrate upon impact, thus raising the substrate temperature. Consequently, the partially (or fully) solidified droplets are heated up to the temperature of the substrate / deposition zone, which leads to a partial re-melting or dissolution of the primary α-Al phase, for the partially solidified droplets, and the eutectic structure for the fully solidified droplets. Consequently, the solidification time / interval is lengthened so that even though there is a fast heat extraction from the substrate / deposition zone by the cooling gas, the primary α-Al phase grows coarse (as compared to microstructure of droplets that solidified entirely in the gas), following the Gulliver-Scheil solidification mode, until the eutectic temperature is reached.

An undercooled eutectic structure is thus formed at the grain boundaries around the primary α-Al phase. The reason why the eutectic undercooling in powders and SD are similar was described in the Introduction and in [12]. The semi-solid droplets are encased in a thin layer of aluminum oxide. The $\theta - Al_2Cu$ phase of the eutectic must nucleate inside of each of these, whether droplet or flattened droplet on the substrate. Note in SD each of these flattened droplets nucleates its own $\theta - Al_2Cu$ phase independent of the adjacent ones due to their separation by an oxide layer. This phenomenon was termed ‘slushy balloon’ in [12].

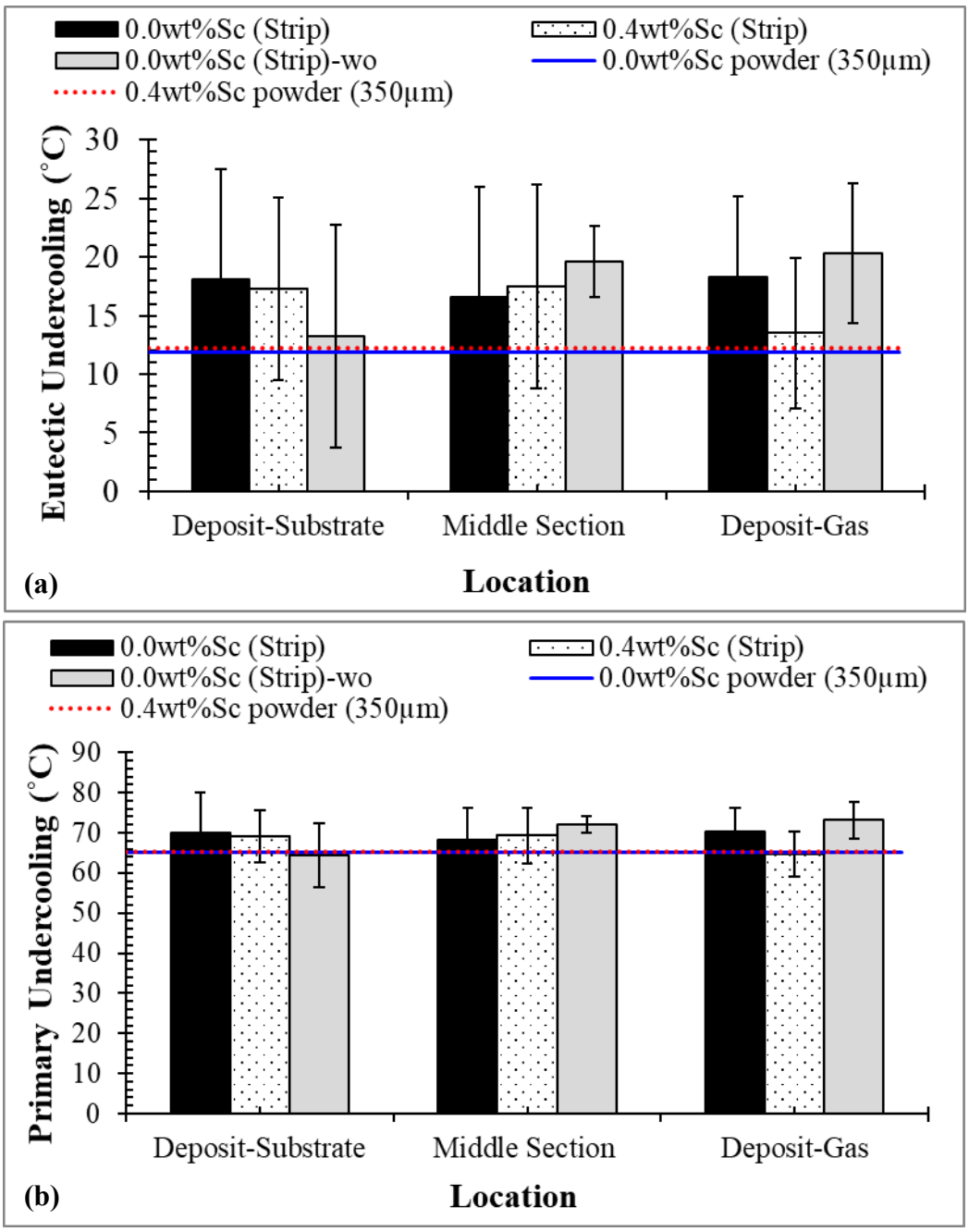

Figure 7: Eutectic (a) and primary (b) nucleation undercooling variation at different location on the sample cross section along Z-axis, compared with powders of equivalent size for the two investigated Al-4.5wt%Cu-xSc (x=0.0wt%Sc and x=0.4wt%Sc) alloys

This work has so far demonstrated a successful atomization of hypoeutectic binary Al-Cu and ternary Al-Cu-Sc alloy into spherical powders and SD strips, and their subsequent characterization. Sc is a unique alloying addition to aluminum alloys in that it forms a very

stable Al_3Sc phase whose size and distribution, after heat treatment (age hardening/ageing), makes it ideal for the pinning of dislocations during plastic deformation [18]. The effect is so strong that it can add more than 200MPa to the yield strength of many aluminum alloys, including Al-4.5wt%Cu as demonstrated in our previous work. The high cooling rate enhances the solid solubility of Sc in aluminum and on a subsequent heat treatment a greater strengthening is achieved [19] [28].

While Al-4.5wt% Cu is a well-characterized alloy for which the relationship between solidification rate and interdendritic spacings are well-known, the rapid solidification developed microstructures observed in this work demonstrated that a small Sc addition (0.4wt%) has a negligible effect upon the as solidified structures.

3.4.1. Aging treatment

In a previous publication [19], nano-precipitates of Sc were observed in the matrix of Al - 4.5 wt% Cu-0.4 wt% Sc powders, following the aging treatment. These precipitates were deemed to be responsible for the dramatic increase in Vickers microhardness, up to 120 HV, equivalent to a yield stress of ~250 MPa which represents an increase of about 100 MPa in yield stress relative to an Al-4.5 wt% Cu sample that underwent a classical T6 heat treatment procedure (solutionizing, quenching, and aging).

Figure 8a and 8b show respectively the Vickers macrohardness (HV) and corresponding yield stress (YS) results of as-atomized as well as aged (300°C for 20hrs) powders and SD samples for both Al-4wt%Cu (Al-Cu) and Al-4wt%Cu-0.4wt%Sc (Al-Cu-Sc). As can be seen, aging treatment at 300°C for 20hrs, yields an increase in the mechanical properties of the Sc-containing sample (Al-Cu-Sc_Aged), while there is a decrease in the properties of the Al-Cu samples (Al-Cu_Aged).

The decrease in HV / YS of the Al-Cu samples after aging is due to the depletion of the α-Al solid solution of Cu atoms by diffusion to the grain boundaries, as evidenced by the SEM micrographs shown in Figure 9a, and described in Figure 9b. It is worth noting that the root-mean-square (RMS) diffusion distance of Cu in Al, calculated following the steps

described in [19], is 2.6 μm at 300°C after 20hrs. This distance is too short for Cu atoms that are located in the middle of a pro-eutectic α-Al to move out of the cell, but it is enough for the supersaturated Cu atoms which are located at the periphery of the pro-eutectic α-Al to be at the cell boundaries (the measured average cell size is 24±5 μm).

As for the increase in HV / YS of the SD Al-Cu-Sc (Al-Cu-Sc_Aged) samples following the aging treatment, Figure 10a and 10b show evidence of Sc-rich sub-micron-precipitates within the α-Al matrix, following the heat treatment. These precipitates were not observed within the primary phase prior to aging. It was demonstrated in previous work [20] that the RMS diffusion distance for Sc is 192 nm when aged for 20 hours at 300ºC. Thus, prior to aging, the Sc must be super-saturated in the primary matrix. It is worth noting that the hardness results for the powders heat treated under similar conditions (300°C for 20hrs), Al-Cu-Sc_Aged_ Powder, show a higher hardness of 120HV (Figure 8a) as compared to the investigated SD samples with a hardness value of 92HV (Figure 8a). This lower hardness of the investigated SD Al-4.5 wt% Cu-0.4 wt% Sc in He, after aging for 20hrs at 300°C, compared to the powders processed under the same conditions could be explained by a combination of facts that are shown in Figure 10a: (i) the primary α-Al phase in the microstructure of the SD samples is coarser relative to powders microstructure (indeed, it is shown in section 3.2 that the cell spacings of the strips are one order of magnitude larger than those of the powders in this investigation), and (ii) the Al_3Sc precipitates in the aged SD Samples *(AlCu-Sc_Aged)* are also relatively coarse. In addition, EBSD observations (Figure 11), show evidence of formation of W-phases. The W-phase, having a $ThMn_{12}$-type structure, is reported to have a unit-cell parameters of a=0.863nm and c= 0.510 nm[32]. It has been also shown that the W phase decreases the mechanical properties of hypoeutectic Al-Cu-Sc alloys compared to those of Al-Cu [32-34]. The latter study involved the casting, hot and cold deformation of the ingots as well as the heat treatment of the alloys. The authors showed that the UTS and YS of 0.4wt%Sc containing alloys decreased by about 10% compared to the binary Al-4Cu alloy. Figure 10 does show some small sub-micron sized precipitates that may be the θ phase or θ' phase. But they are coarser and fewer than the surrounding Sc containing precipitates. We can only, therefore,

conclude that the strengthening in aged SD samples is due to these many Sc containing precipitates within the primary α-Al phase that are void of Cu, and hence not the W phase.

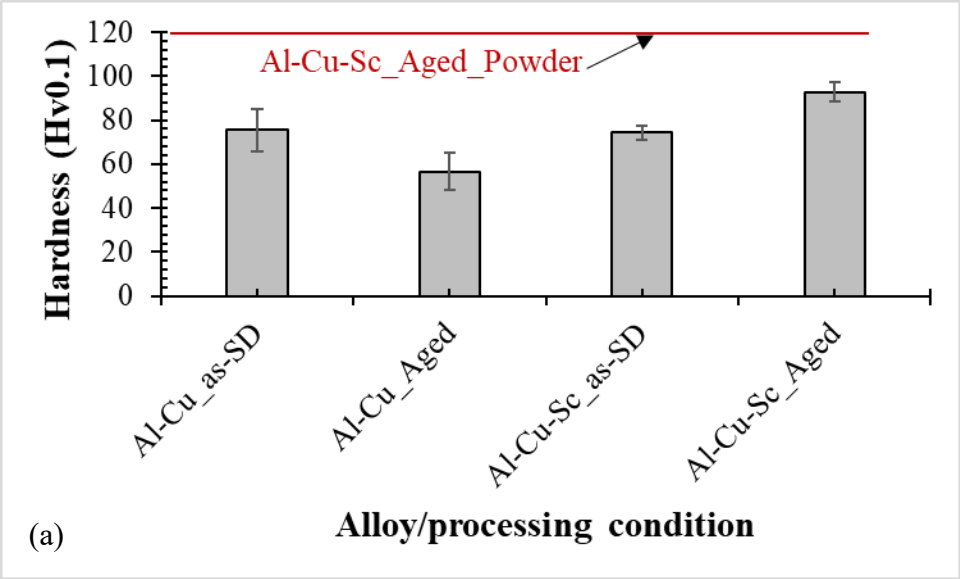

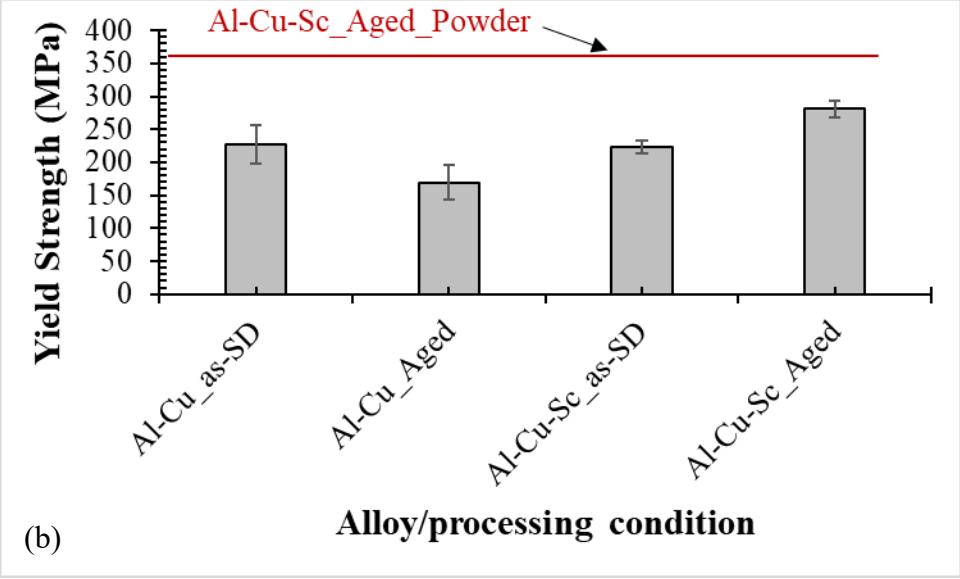

Figure 8: (a) Hardness (b) Yield strength of the two investigated Al-4.5wt%Cu-xSc (x=0.0wt%Sc and x=0.4wt%Sc) alloys powders and strips/spray deposits (SD)

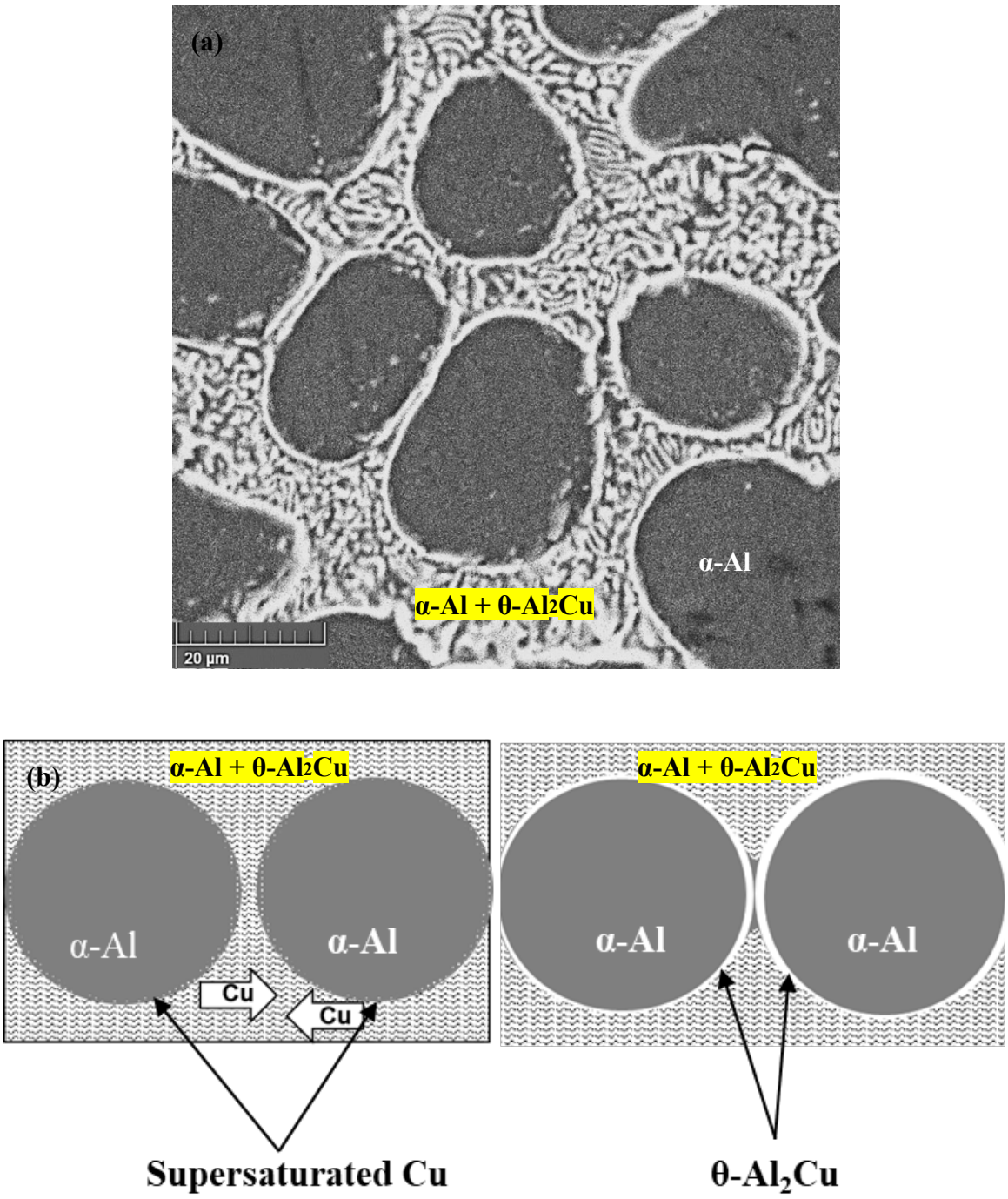

Figure 9: (a) SEM BSE images of a SD Al-4.5 wt% Cu in He, after aging for 20hrs at 300C, showing primary α-Al cells (dark) surrounded by Cu-rich boundaries (white) at the interface with the irregular eutectic (α-Al +θ-Al_2Cu) structures (b) Schematic of the pathways (during ageing treatment) for the formation of the Cu-rich boundaries at the interface α-Al cells-eutectic structure. The observed irregular eutectic structure results from the solid-state diffusion of Cu, and Al during aging treatment.

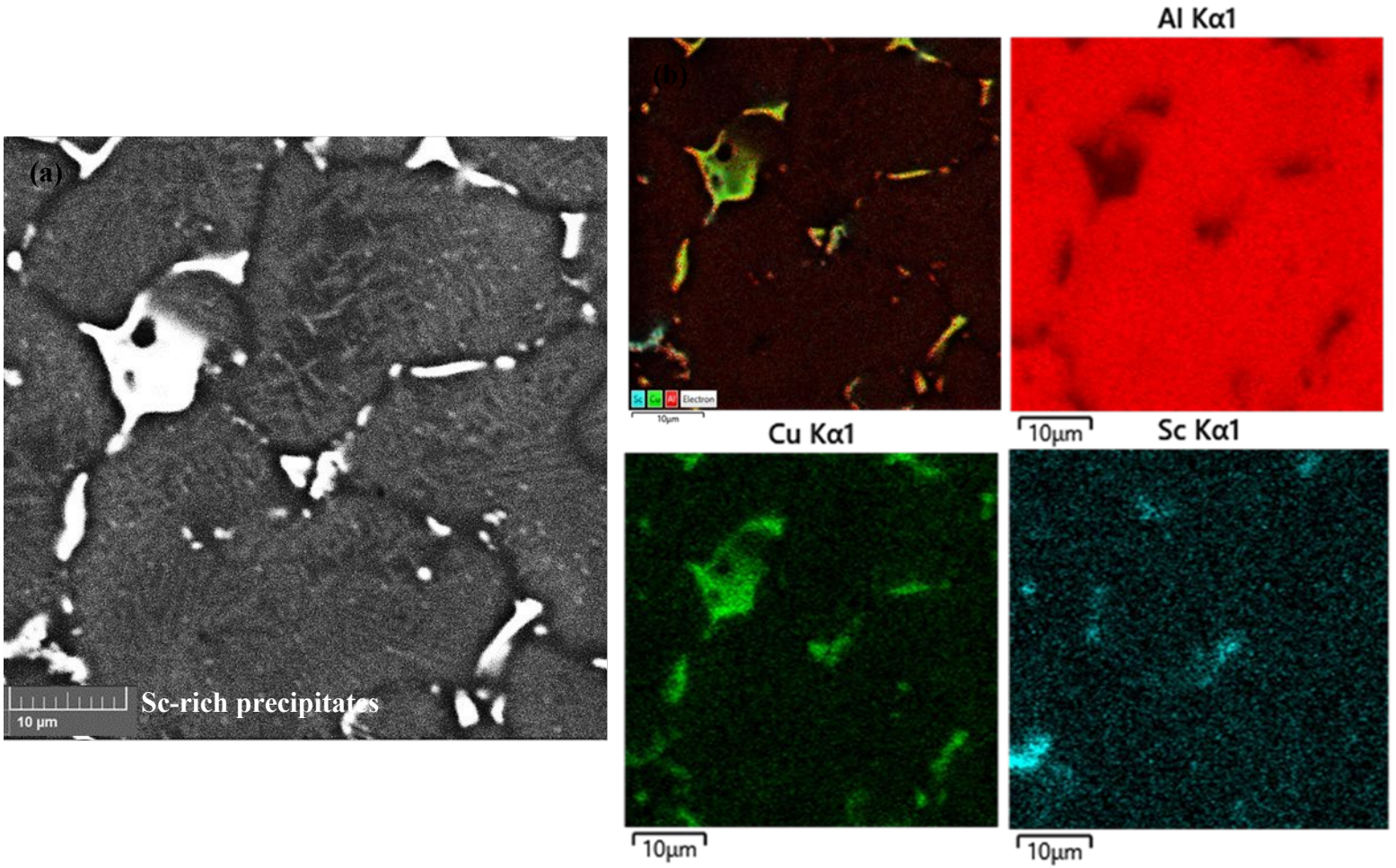

Figure 10: (a) SEM BSE images of a SD Al-4.5 wt% Cu-0.4 wt% Sc in He, after aging for 20hrs at 300C, showing sub-micron-precipitates within the primary α-Al cells surrounded by Cu-rich boundaries (b) EDS map of Al, Cu and Sc within the microstructure.

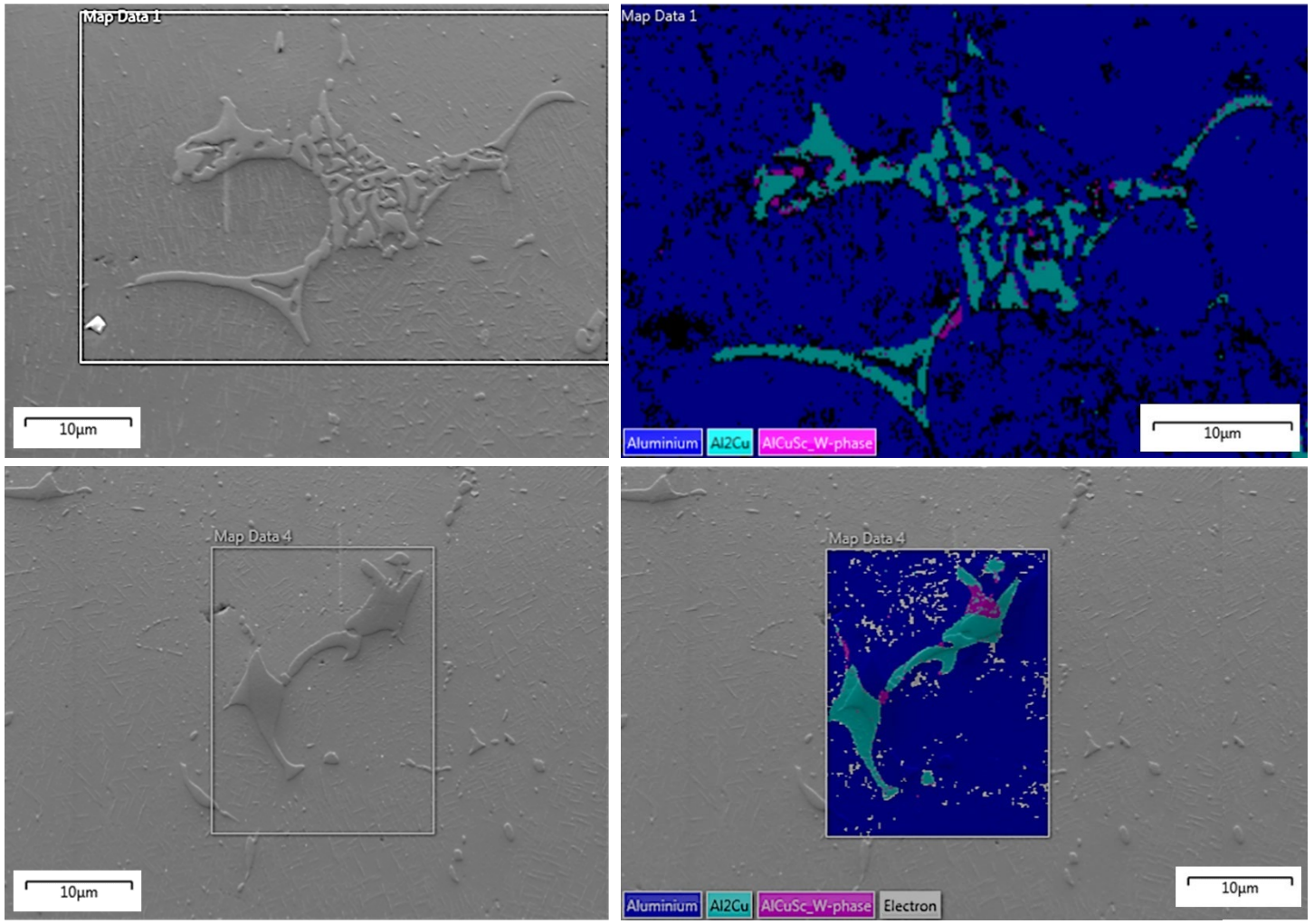

Figure 11: Electron backscatter diffraction (EBSD) maps recorded in two regions of the aged SD Al-4.5wt%Cu-0.4wt% Sc at 300ºC for 20hrs (Al-Cu-Sc_Aged) showing the presence of the W phase.

While coarsening of the primary phase occurred during the microstructure formation, coarsening of the Al_3Sc precipitates must have occurred during aging treatment of the powders and SD. However, both powders and SD samples were aged under similar conditions (300°C for 20hrs), therefore, sub-micron-precipitates of Al_3Sc must have already nucleated during spray deposition (induced by semi-liquid deposition induced reheating), so that, during the aging treatment, these already nucleated Al_3Sc, coarsened.

4. Summary and Conclusions

Impulse Atomization (IA) successfully generated rapidly solidified hypoeutectic Al-4.5 wt% xSc (x= 0.0, and 0.4 wt% Sc) powders and strips (by spray Deposition (SD)) in Ar atmosphere. Copper substrates with and without oil coating were used for SD. The investigations of both alloys in powder as well as strip forms lead to the following conclusions;

- ✓ Oil coated substrate is found to yield faster heat dissipation due to a better substrate-deposit contact.
- ✓ Powders primary phase microstructures are found to be finer than their corresponding strips although copper heat conductivity is much higher than Ar. Indeed, the micron size powders fully solidified by losing heat to the Ar atmosphere, without any significant increase in the temperature of the gas. Whereas, during SD, the droplets, partially solidify in the gas. Deposition of subsequent layers leads to partial re-melting or dissolution of the primary α-Al phase and results in coarsening.
- ✓ The eutectic fractions in powders and SD of the Al-Cu alloys are the same, suggesting that eutectic fraction is nucleation undercooling dependent rather than solidification cooling rate.
- ✓ The eutectic undercooling does not vary with solidification cooling rate. SD yields a somewhat higher eutectic undercooling as compared to powders. Because when they land on the copper substrate, the partially solidified droplets in SD must experience further cooling before they reach the eutectic composition. Therefore, the thermal cooling rate of the strip gets slowed down leading to a lower eutectic

nucleation temperature as compared to powders that solidified completely in the argon atmosphere.

- ✓ The primary undercooling is the same for both IA powders and SD samples regardless of the nature of the deposition substrate. This is due to the primary nucleation occurring before the spray impacts the substrate, so that droplets of the same size experience similar primary nucleation undercooling in both powder, and strips.
- ✓ Within the limits of the measurements in this investigation, the effect of Sc was not discernible on solidified primary α-Al.
- ✓ Direct aging of Sc-containing samples show an increase in hardness due to sub-micron

  precipitations of Sc-rich phases with the primary α-Al matrix.
- ✓ The hardness of aged Al-Cu-Sc powders (300°C for 20hrs), is found to be superior to the hardness of the aged SD Al-Cu-Sc under similar conditions. This is attributed to a combination of factors (i) the primary α-Al phase is coarser for the aged SD Al-Cu-Sc alloy, and (ii) the Al_3Sc precipitates in the aged SD Al-Cu-Sc samples are also coarser. In addition, *Electron backscatter diffraction (*EBSD) observations showed evidence of formation of W-phase in aged SD Al-Cu-Sc microstructure, which are reported to decrease mechanical properties of hypoeutectic Al-Cu-Sc alloys.

Acknowledgements

The authors express their gratitude to Dr. Jonas Valloton for the EBSD results, and to the Electron Microprobe Laboratory in the Department of Earth and Atmospheric Sciences, University of Alberta. The Natural Sciences and Engineering Research Council (NSERC) of Canada is gratefully acknowledged for their financial support and the support of the NSERC-HI-AM for partial support of one of the co-authors (A-A B) in the preparation of this manuscript.

References

[1] M. C. Flemings, Solidification Processing, London: McGraw-Hill, 1974.

[2] M. H. Dieter, M. M. Douglas, Editors, Solidification of Containless Undercooled Melts, Germany, Wiley-VCH, 2012.

[3] N. Ellendt, R.-R. Schmidt, J. Knabe and H. Henein, "Spray Deposition using Impluse Atomization Technique," *Materials Science and Engineering:A,* vol. 1, no. 383, pp. 107-113, 2004.

[4] J. B. Wiskel, K. Navel, H. Henein and E. Maire, "Solidification study of aluminum alloys using Impulse Atomization: Part I: Heat Transfer Analysis of An Atomized Droplet," *Canadian Metallurgical Quarterly,* vol. 41, no. 2, pp. 97-110, 2002.

[5] J. B. Wiskel, K. Navel, H. Henein and E. Maire, "Solidifcation Study of Aluminum Alloys using Impulse Atomization: Part II. Effect of Cooling Rate on Microstructure," *Canadian Metallurgical Quarterly,* vol. 41, no. 2, pp. 193-204, 2002.

[6] H. Henein, "Single Fluid Atomization Through the Application of Impulse to a Melt," *Materials Science and Engineering A,* no. 326, pp. 92-100, 2002.

[7] J. Chen, U. Dahlborg, C. M. Bao, M. Calvo-Dahlborg and H. Henein, "Microstructure Evolution of Atomized Al-0.6wt%Fe and Al-1.90wt%Fe Alloys," *Metallurgical and Materials Transactions B,* vol. 42, no. 3, pp. 557-567, 2011.

[8] P. Delshad Khatibi, A. B. Phillion and H. Henein, "Microstructural Investigation of D2 Tool Steel during Rapid Solidification," *Powder Metallurgy,* vol. 57, no. 1, pp. 70-78, 2013.

[9] A. Ilbagi and H. Henein, "3D Quantitative Characterization of Rapidly Solidified Al-36wt%Ni," *Metallurgical Transactions A,* vol. 45, no. 4, pp. 2152-2160, 2014.

[10] N. Ciftci, N. Ellendt, R. Von Bargen, H. Henein, L. Mädler and V. Uhlenwinkel, "Atomization and Characterization of a Glass Forming Alloy," *Journal of NonCrystalline Solids,* vol. 36, no. 42, pp. 394-395, 2014.

[11] A.-A. Bogno, J. E. Spinelli, C. R. Afonso and H. Henein, "Microstructural and Mechanical Properties Analysis of Extruded Sn-0.7Cu Solder Alloy," *Journal of Materials Research and Technology,* vol. 4, no. 1, pp. 84-92, 2015.

[12] I. T. Chang, B. Cantor and A. G. Cullis, "Metastable Ge-Sn Alloy Layers Prepared by Pulsed Laser Melting," *MRS Online Proceeding Library Archive,* vol. 407, p. 157, 1989.

[13] I. T. H. Chang, P. Svec, M. Gogebakan and B. Cantor, "Rapidly Solidified Al 85 Ni 15-x Y x (x=5,8,10) Alloys," *Materials Science Forum,* vol. 225–227, p. 335–340, 1996.

[14] C. R. Ho and B. Cantor, "Heterogeneous nucleation of solidification of Si in Al-Si and Al-Si-P alloys," *Acta Metallurgica et Materialia,* vol. 43, no. 8, pp. 32313246, 1995.

[15] D. Siemiaszko, B. Kowalska, P. Jóźwik and M. Kwiatkowska, "The Effect of Oxygen Partial Pressure on Microstructure and Properties of Fe40Al Alloy Sintered under Vacuum," *Materials (Basel),* vol. 8, no. 4, pp. 1513-1525, 2015.

[16] H. Henein, "Why is spray forming a rapid solidification process," Mat.-wiss. u.Werkstofftech*,* 41 (7), pp. 555-561, 2010.

[17] S. Yin, A.-A. Bogno, H. henein and M. Gallerneault, "On the Roleof Sc in Powders and Spray Deposits of Hypoeutectic Al-Mg Alloys, *J. Phase Equilibrium and Diffusion,* https://doi.org/10.1007/s11669-021-00934-5, 2022, 12 pages.

[18] I. Polmear, Light Alloys -- Metallurgy of Light Metals 3rd ed., London: Arnold, 1995.

[19] V. L. Elagin, V. V. Zakharov and T. D. Rostove, "Scandium-alloyed aluminum alloys," *Metal Science and Heat Treatment,* vol. 34, no. 1, pp. 37-45, 1992.

[20] A.-A. Bogno, H. Henein, D. G. Ivey, J. Valloton, G. Reinhart, D. Sediako and M. Gallerneault, "Effects of Scandium on Rapid Solidified Hypo-eutetic Aluminum Copper," *Canadian Metallurgical Quarterly,* vol. 59, no. 1, pp. 101-115, 2020.

[21] M. Sohi, "Aging Behavior of Flexcast Al-Mg Alloys with Sc and Zr Additions," The University of British Columbia, Vancouver, MASc thesis, 2012.

[22] E. A. Marquis, D. N. Seidman and D. C. Dunand, "Effect of Mg addition on the creep and yield behavior of an Al-Sc alloy," *Act Materialia,* vol. 51, pp. 47514760, 2003.

[23] Prasad, A (2006). Microsegragation studies of rapidly solidified binary Al-Cu alloys (Doctoral dissertation, University of Alberta, Edmonton, AB, Canada). ProQuest Dissertations Publishing, NR14028.

[24] A-A. Bogno, P. Natzke, S. Yin, H. Henein, Undercooling of rapidly solidified droplets and spray formed strips of A1-Cu (Sc), Proceedings of Characterization of Minerals, Metals and Materials 2015, J. Carpenter et al, Eds., TMS 2015, 8 pages, March 15-19, 2015.

[25] E. J. Arbtin and G. Murphy, "Correlation of Vickers hardness number, modulus of elasticity, and the yield strength for ductile metals," *Ames Laboratory ISC Technical Reports,* p. 50, 1953.

[26] W. Hearn, A.-A. Bogno, J. E. Spinelli, J. Valloton and H. Henein, "Microstructure Solidification Maps for Al-10wt%Si Alloys," *Metallurgical and Materials Transactions A ,* vol. 50, no. 3, pp. 1333-1345, 2019.

[27] E. A. Brandes and G. B. Brooks, in *Smithells metals reference book*, London, Butterworths-Heinemann, 1998, pp. 14(1) - 14(4).

[28] A. A. Bogno, P. D. Khatibi, C. A. Gandin and H. Henein, "Quantification of dendritic and eutectic nucleation undercoolings in rapidly solidified hypoeutectic Al-Cu droplets," *Metall. Mater. Trans. A, 47A, 4606-4615,* 2016.

[29] S. Haferl and D. Poulikakos, "Transport and solidification phenomena in molten microdroplet pileup," *Journal of Applied Physics,* vol. 92, no. 3, pp. 1675-1689, 2002.

[30] A. A. Bogno, H. Henein and M. Gallerneault, "Design and Processing Conditions of Hypoeutectic Al-Cu-Sc Alloys for Maximum Benefit of Scandium," *Light Metals,* pp. 1609-1616, 2018.

[31] J. Valloton, A.-A. Bogno, and H. Henein, "Scandium Effect on Undercooling and Dendrite Morphology of Al-4.5 Wt Pct Cu Droplets", Metallurgical and Materials

Transactions A: Physical Metallurgy and Materials Science, vol. 50A, pp. 5700-5706, 2019.

[32] J.O. Andersson, T. Helander L. Höglund et al. "Thermo-Calc and Dictra, Computational Tools for Materials Science," Calphad, 26, 273–312, 2002.

[33] G.F. Xu, Z.R. Nie, T.N. Jin, L. Rong, H.Q. Ruan and Z.M. Yin, "Microstructure and Properties of Al-4Cu alloy containing Sc, Transactions of Nonferrous Metals Society of China, 14(1), 63-66, 2004.

[34] X. Guo, N. Zuo, J. Tour, R. Li, R. Har and Y. Zhi, "Microstructure and Properties of Al-4Cu alloy containing Sc," Transactions of Nonferrous Met. Society of China, 14(1), 63-66, 2004.